Supporting Information

Ultrafine rhenium-ruthenium nanoparticles decorated on functionalized carbon nanotubes for simultaneous determination of antibiotic (nitrofurantoin) and anti-testosterone (flutamide) drug†

Pitchaimani Veerakumar,[*ab] Venkatachalam Vinothkumar,[c] Shen-Ming Chen,[*c] Arumugam Sangili,[c] King-Chuen Lin,[*ab]

[a]Department of Chemistry, National Taiwan University, No. 1, Roosevelt Road, Section 4, Taipei, 10617, Taiwan

[b]Institute of Atomic and Molecular Sciences, Academia Sinica, No. 1, Roosevelt Road, Section 4, Taipei, 10617, Taiwan

[c]Department of Chemical Engineering and Biotechnology, College of Engineering, National Taipei University of Technology, No. 1, Chung-Hsiao East Road, Section 3, Taipei 10608, Taiwan

***Corresponding Authors**

E-mail: spveerakumar@gmail.com (P. Veerakumar); Tel.: +886-2-23668230; Fax: +886-2-23620200

E-mail: smchen78@ms15.hinet.net (S.-M. Chen); Fax: +886-2-27025238; Tel: +886-2-27017147

E-mail: kclin@ntu.edu.tw (K.-C. Lin); Tel.: +886-2-33661162; Fax: +886-2-23621483

Preparation of *f*-MWCNT

The as-received pristine MWCNT were treated with a mixture of 3:1 concentrated H_2SO_4 and HNO_3 by volume under stirring for 6 h at 60 °C, kept to sit for another 12 h and then stirred for 2 h at the same temperature.[S1] Subsequently, the solution was diluted with DI water and left overnight. The mixture was vacuum filtered and washed with distilled water repeatedly until neutral pH. Finally, the functionalized MWCNT was dried for 12 h at 90 °C and named as "*f*-MWCNT".

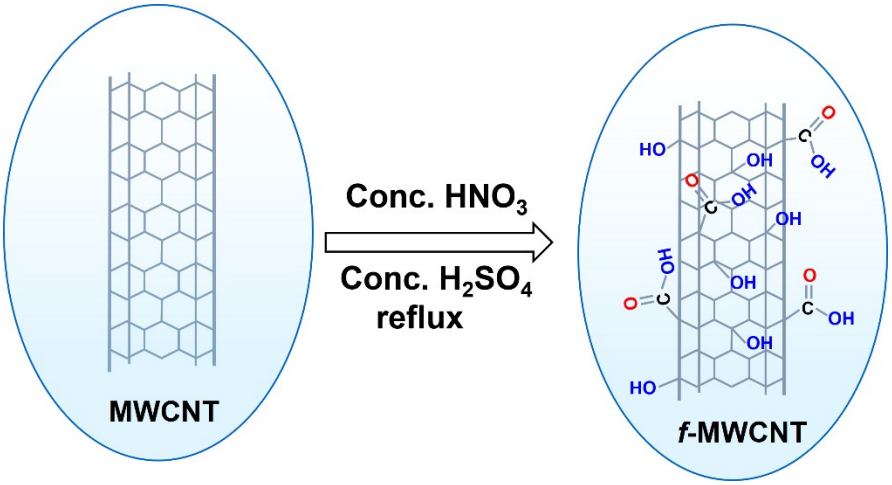

Fig. S1. The preparation of *f*-MWCNT.

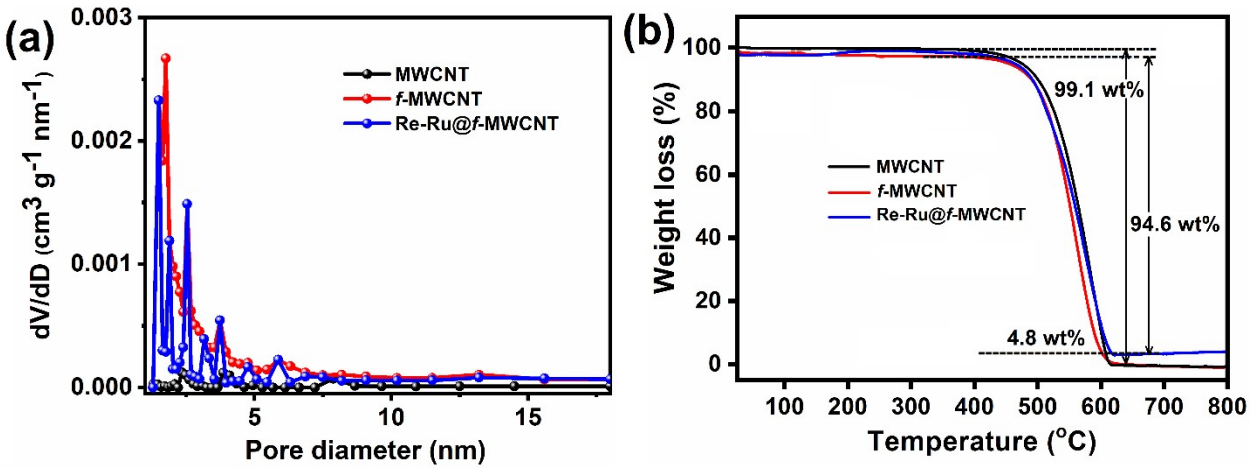

Fig. S2. The pore size distributions and (b) TGA curves of pristine MWCNT, *f*-MWCNT, and Re-Ru@*f*-MWCNT samples.

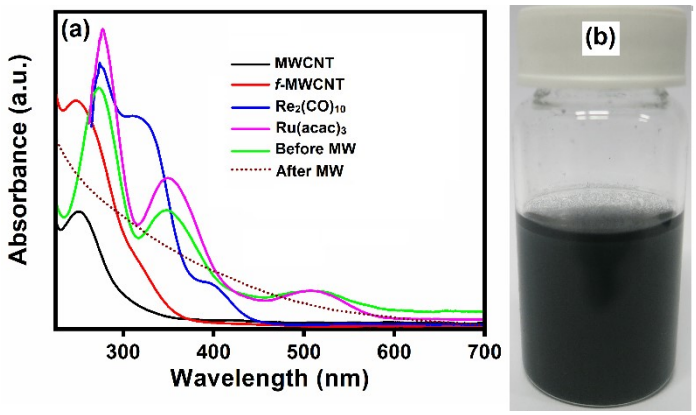

Fig. S3. (a) UV-vis absorption spectra of the pristine MWCNT, *f*-MWCNT, $Re_2(CO)_{10}$, $Ru(acac)_3$, before and after MW irradiation and (b) Dispersion in aqueous media of Ru@*f*-MWCNT for 48 h.

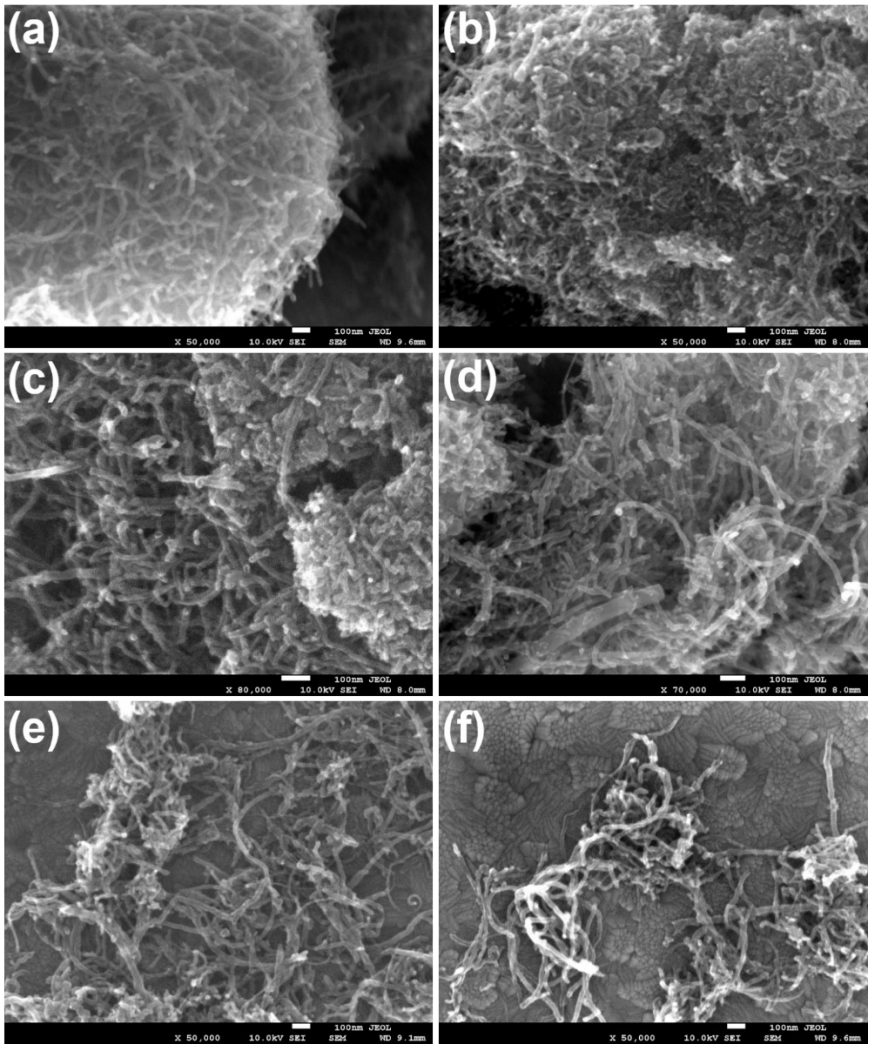

Fig. S4. FE-SEM images of (a) pristine MWCNT, (b) *f*-MWCNT (c) Ru@*f*-MWCNT T composite with different magnification.

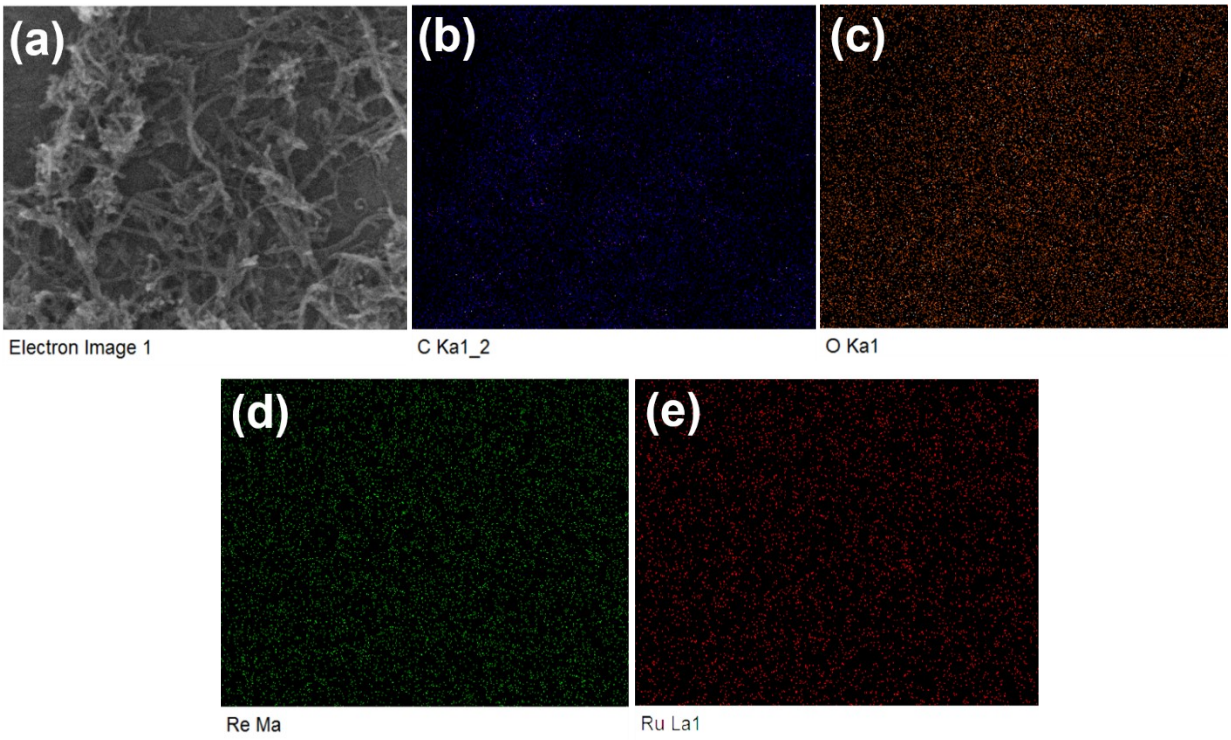

Fig. S5. (a) FE-SEM image of Ru@*f*-MWCNT composite, (b-f) EDS elemental mapping region of (b) C, (c) O, (d) Re, and (e) Ru.

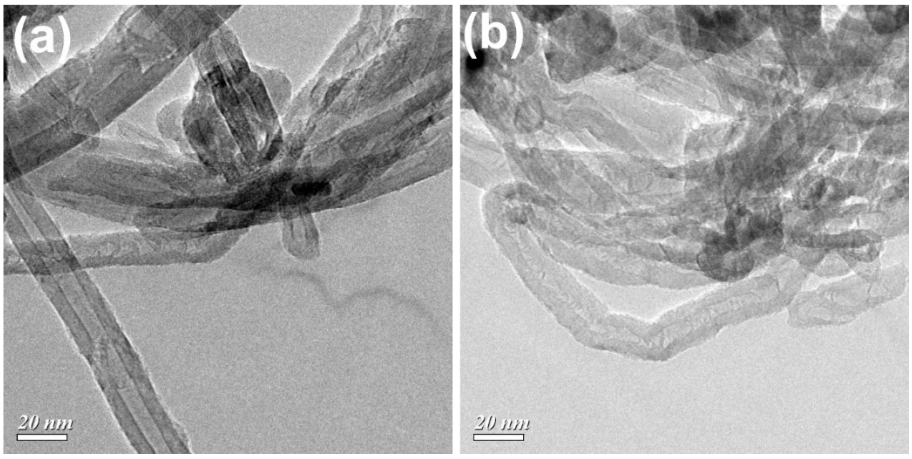

Fig. S6. FE-TEM image of (a) pristine MWCNT and (b) *f*-MWCNTs.

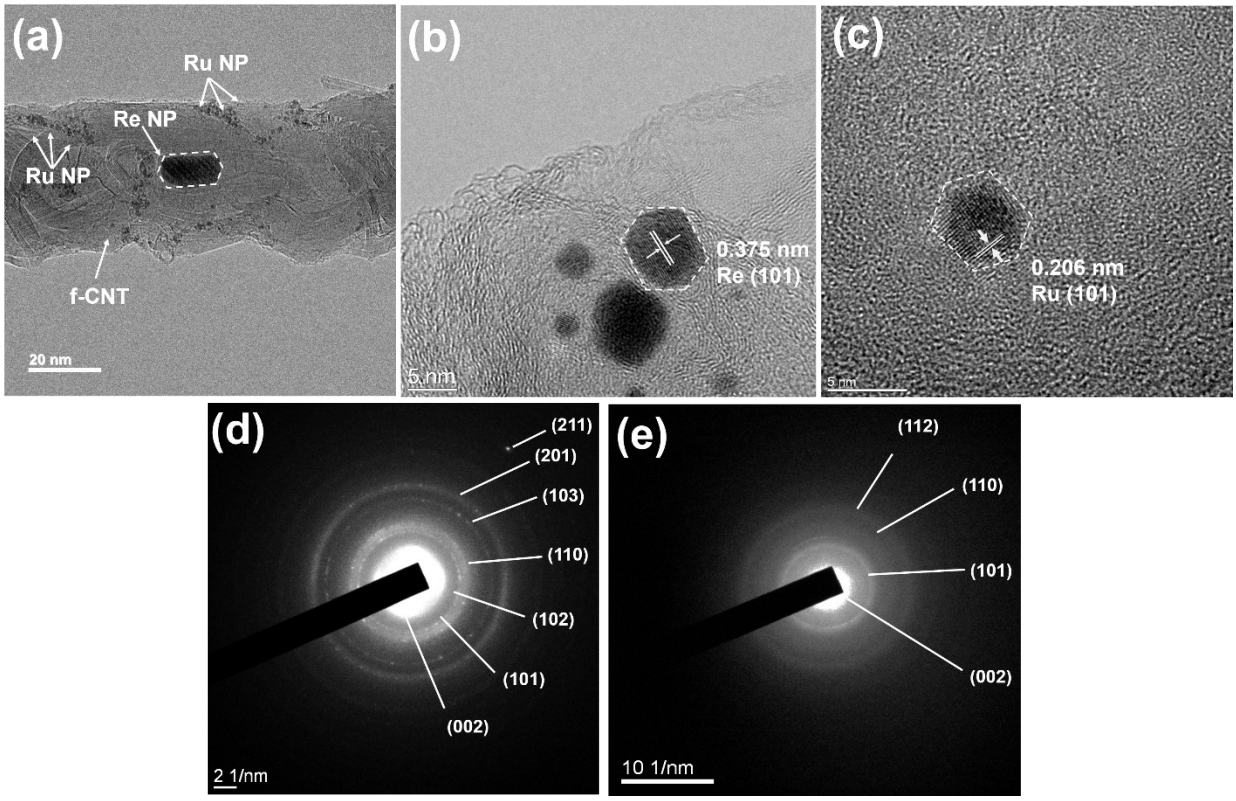

Fig. S7. FE-TEM image of (a) Ru@*f*-MWCNT composite, (b,c) FE-TEM images of Re NP and Ru NP, and (d,e) SEAD patterns.

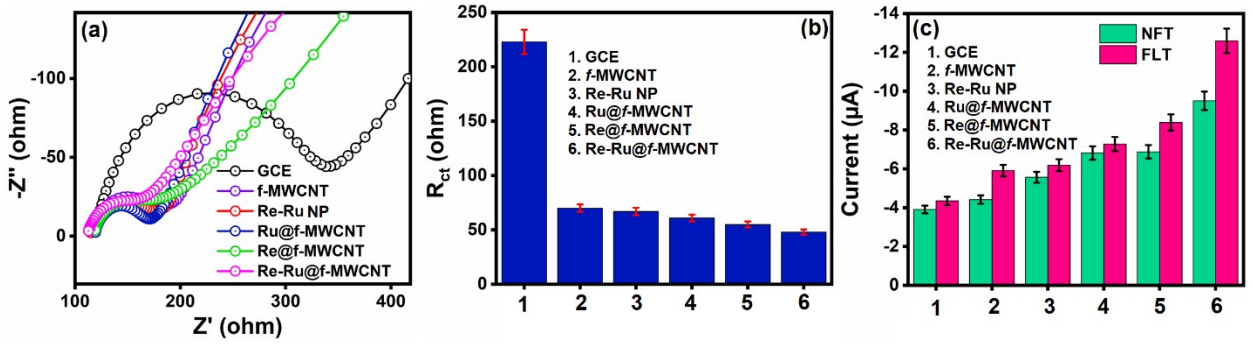

Fig. S8. (a) The enlarged view of EIS plots, (B) bar diagram of modified electrodes *vs* charge transfer resistance (R_{ct}), and (c) electroreduction current for simultaneous detection of 100 μM of NFT and FLT in the presence of (1) bare GCE, (2) *f*-MWCNT/GCE, (3) Re-Ru NP/GCE, (4)

Ru@*f*-MWCNT/GCE, (5) Re@*f*-MWCNT/GCE, and (6) Re-Ru@*f*-MWCNT/GCE containing 0.05 M PB (pH 7.0) at 50 mV s^{-1}.

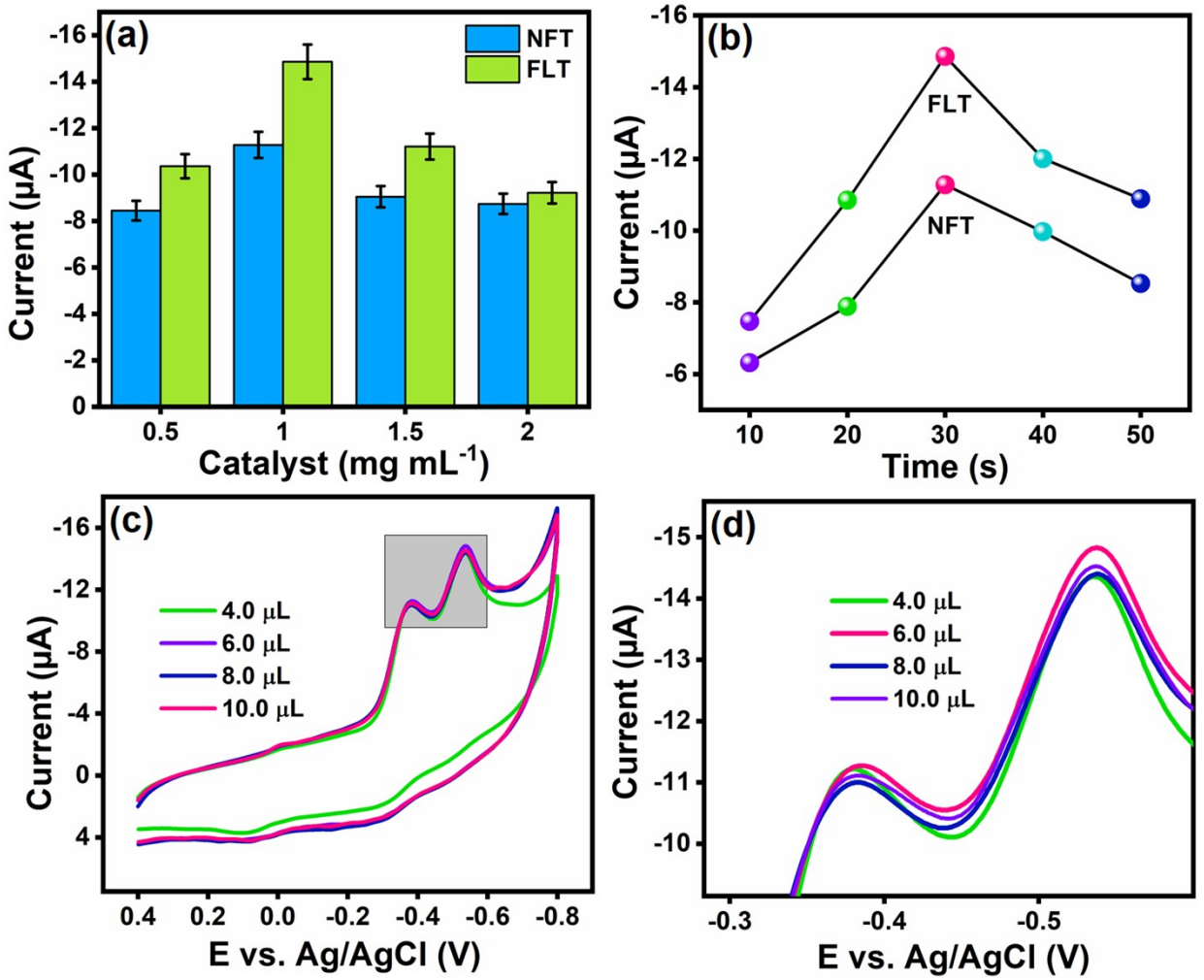

Fig. S9. (a) The plot against catalyst dosage *vs* reduction peak current, (b) The influence of accumulation time on the reduction current of Re-Ru@*f*-MWCNT/GCE, (d) CV response of Re-Ru@*f*-MWCNT/GCE with various NFT and FLT concentration, and (e) Their corresponding enlargement view of reduction current. All the measurements were carried out under N_2-saturated in 0.05 M PB (7.0) towards simultaneous detection of 100 μM NFT and FLT.

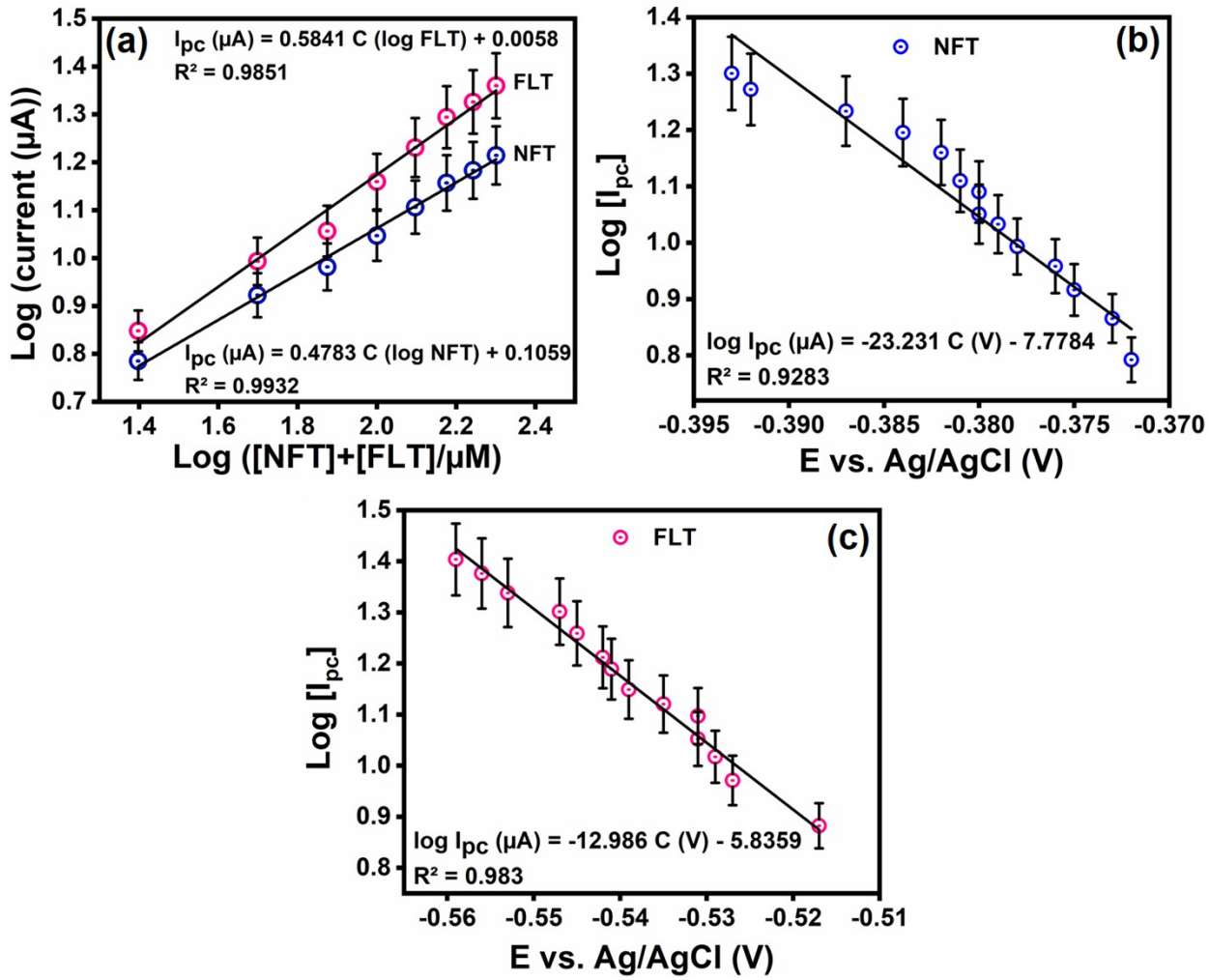

Fig. S10. (a) The linear plot between the logarithm of reduction peak current and logarithm of concertation, and Tafel plot of the logarithm of reduction peak current *vs* reduction peak potential of (b) NFT and (c) FLT.

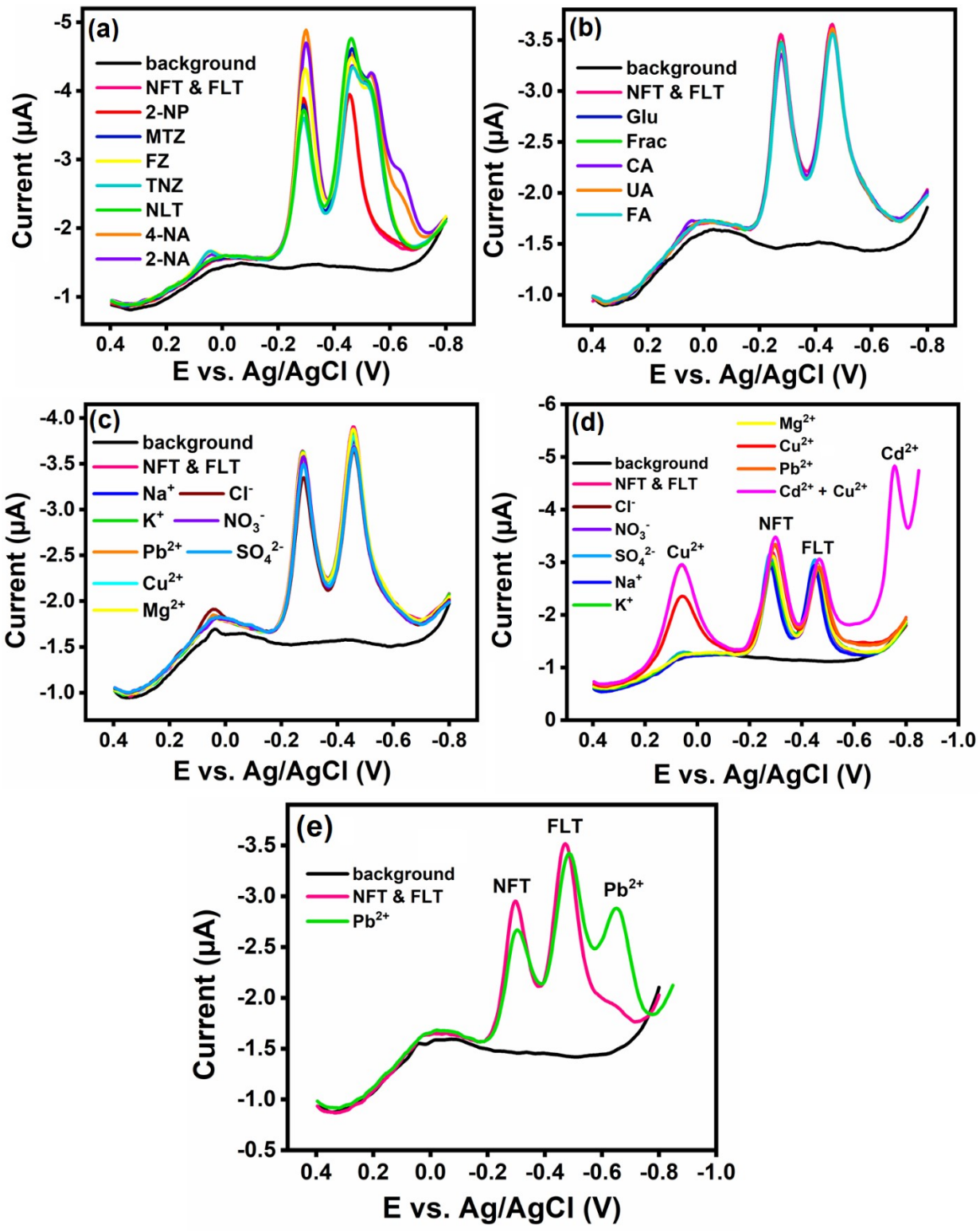

Fig. S11. DPVs of Re-Ru@f-MWCNT/GCE with various interfering species such as (a) nitro molecules, and (b) biological compounds in the simultaneous detection for 25 μM of NFT and 15

μM of FLT, and DPV response for (c) 5-fold, (d,e) 15-fold metal ions in the presence of 20 μM NFT and 10 μM FLT. All the DPV experiments were conducted by 0.05 M PB (pH 7.0).

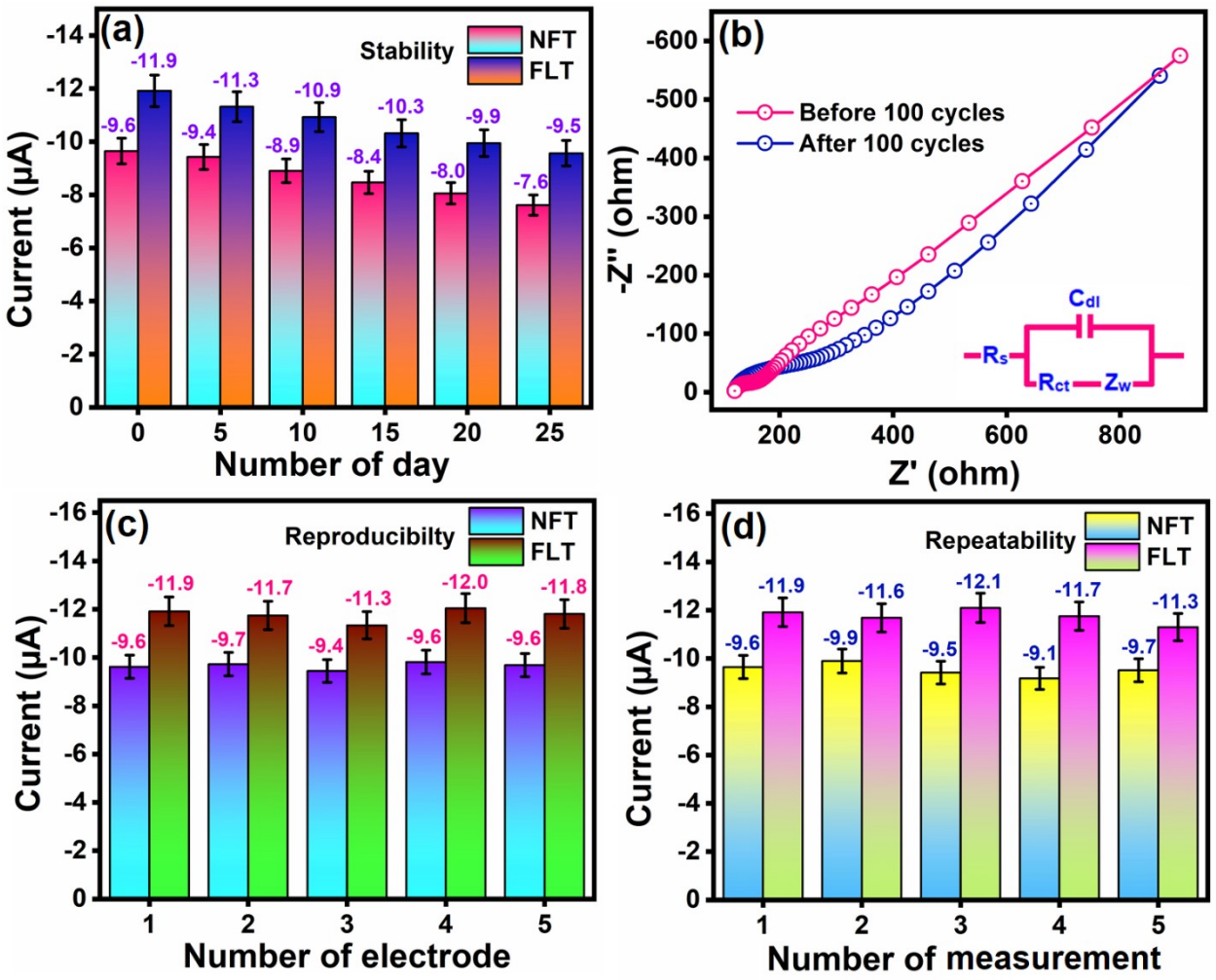

Fig. S12. CV profiles of (a) long-term stability, (b) conductivity, (c) reproducibility, and (d) repeatability on the Re-Ru@*f*-MWCNT/GCE in the nitrogen saturated 0.05 M PB containing pH 7.0 of 75 μM NFT and FLT.

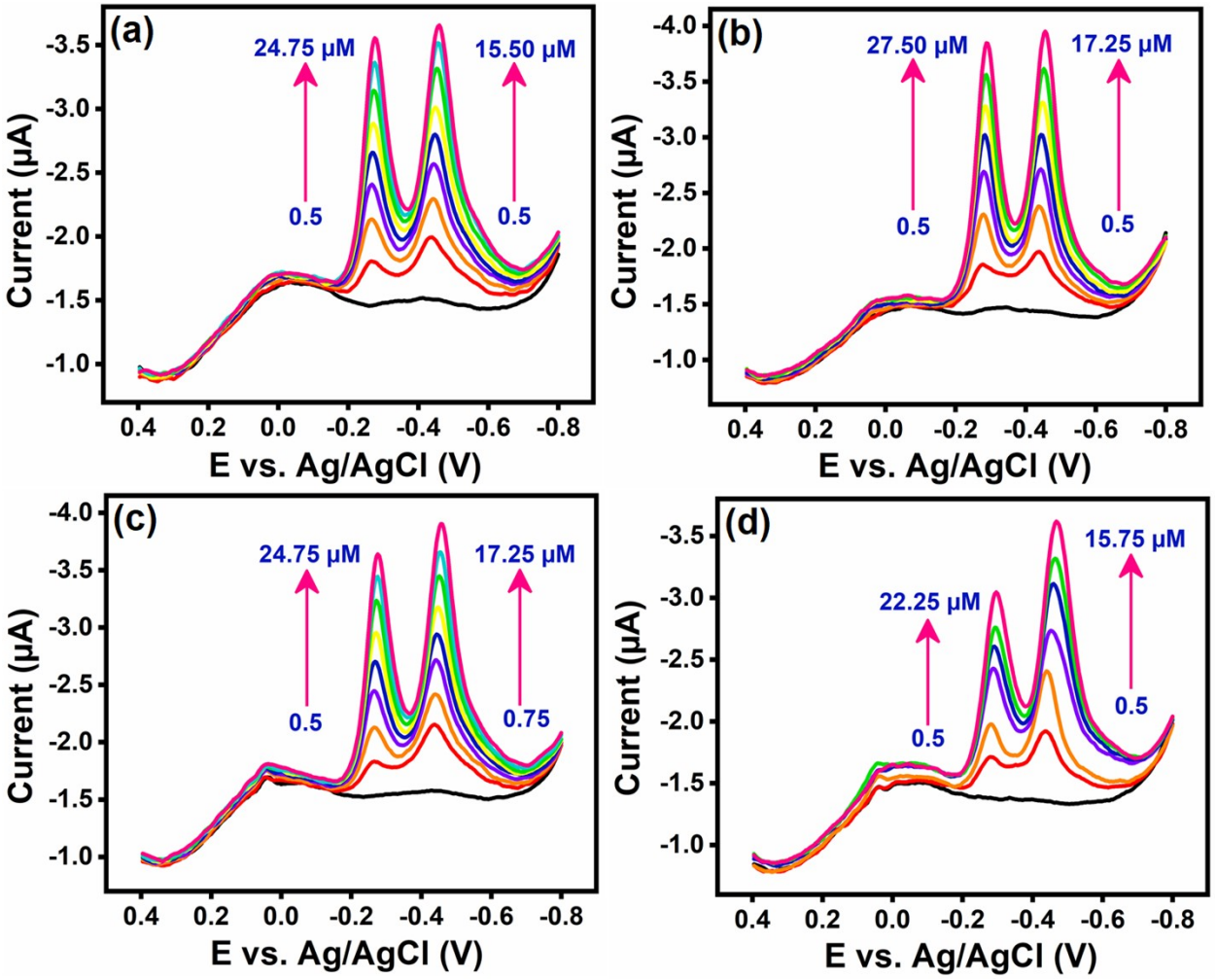

Fig. S13. Simultaneous detection of NFT and FLT in the presence of (a,b) human urine and (c,d) serum real samples were spiked in 0.05 M, PB (pH 7.0) using Re-Ru@*f*-MWCNT/GCE.

Table S1. Textural characteristics for the samples studied.

sample	S_{BET}[a] **($m^2\ g^{-1}$)**	V_{Tot}[a] **($cm^3\ g^{-1}$)**	D_p[b] **(nm)**
MWCNT	113.55 ± 0.05	0.311	2.71
f-MWCNT	223.21 ± 0.05	0.396	3.98
Re-Ru@*f*-MWCNT	186.16 ± 0.03	0.287	3.11

[a]Surface area from BET method and total pore volume (V_{Tot}) calculated at $P/P_0 = 0.99$. [b]Average pore size determined by BJH method.

Table S2. Comparison of the dynamic range and detection limit of different methods for determination of NFT.

Electrodes	Method	WLR (μM)	LOD (nM)	Reference
Extraction urine by supercritical fluids	HPLC[d]	10.9–378.0	12100	S2
Urine	Spectroscopy	42.0–210.0	6000	S3
Animal feeds	Flow injection Chemiluminescence	2.0–23.0	1000	S4
CuNCs[a]	Photoluminescence	0.05–4.0	30	S5
CuNCs[b]	Fluorescence	5–120	730	S6
ZTMOF-1[c]	Quenching luminescence	0–40	175	S7
Re-Ru@f-MWCNT/GCE	Electrochemical	0.04–838.95	4.74	This work

[a]Adenosine-stabilized copper nanoclusters. [b]Dopamine-protected copper nanoclusters. [c]Terpyridine-based zinc metal–organic frameworks with the phenyl and pyridine rings. [d]High performance liquid chromatography.

Table S3. Comparison of the dynamic range and detection limit of different methods for determination of FLT.

Electrodes	Method	WLR (μM)	LOD (nM)	Reference
pespsin-CuNCs[a]	Fluorescent	0.10–100.00	61.82	S8
Au/Ag alloy NPs[b]	Chemiluminescent	0.5–100	12	S9
Protein binding	HPLC/UV[c]	0. 0625–16	15	S10
Pharmaceutical tablets	Flow-injection	100–400	120	S11
Tablets	HPLC	2.9–11.6	–	S12
Fe^{3+}	Spectrophotometric	0.5–10	332	S13
1,10-phenanthroline	Spectrophotometric	0.5–15	726	S13
Re-Ru@f-MWCNT/GCE	Electrochemical	0.04–839.99	3.17	This work

[a]Pepsin protected ultra-small blue fluorescent copper nanoclusters. [b]Silver/gold alloy nanoparticle. [c]High performance liquid chromatography/Ultraviolet visible spectroscopy.

Table S4. DPV profiles of simultaneous detection of NFT and FLT in human urine samples.

Urine samples	Added (μM)		Found (μM)		Recovery(%)		RSD (*n* = 3)	
	NFT	FLT	NFT	FLT	NFT	FLT	NFT	FLT
1	0.50	0.50	0.47	0.49	94.00	98.00	2.69	2.73
2	2.50	1.25	2.46	1.23	98.40	98.40	2.45	2.59
3	4.75	2.50	4.72	2.49	99.36	99.60	2.12	2.28
4	9.75	3.75	9.70	3.72	99.48	99.20	1.93	2.03
5	14.25	5.25	14.19	5.18	99.57	98.66	2.01	1.82
6	18.50	8.50	18.49	8.47	99.94	99.64	1.54	1.37
7	22.50	12.25	22.47	12.22	99.86	99.75	1.39	1.56
8	24.75	15.50	15.43	15.48	99.54	99.87	1.10	1.24
1	0.50	0.50	0.48	0.47	96.00	94.00	2.91	3.09
2	2.75	1.50	2.73	1.48	99.27	98.66	2.73	2.68
3	9.75	2.75	9.67	2.69	99.17	97.81	2.46	2.32
4	15.25	5.25	15.21	5.18	99.73	98.66	2.18	2.14
5	20.50	8.75	20.46	8.72	99.80	99.65	1.98	2.07
6	24.75	12.50	24.71	12.45	99.83	99.60	1.52	1.83
7	29.50	17.25	29.44	17.19	99.79	99.65	1.29	1.65

Table S5. DPV response of simultaneous detection of NFT and FLT in human serum

samples.

Serum samples	Added (μM)		Found (μM)		Recovery (%)		RSD (n = 3)	
	NFT	FLT	NFT	FLT	NFT	FLT	NFT	FLT
1	0.50	0.75	0.48	0.73	96.00	97.33	3.26	3.08
2	2.50	2.75	2.48	2.72	99.20	98.90	2.67	2.91
3	5.25	3.25	5.20	3.22	99.04	99.07	2.82	2.65
4	10.50	4.75	10.47	4.71	99.71	99.15	2.39	2.48
5	15.25	7.50	15.24	7.41	99.93	98.80	2.05	2.17
6	20.75	11.75	20.73	11.70	99.90	99.57	1.95	1.84
7	23.25	15.75	23.22	15.69	99.87	99.61	1.71	1.59
8	24.75	17.25	24.69	17.22	99.75	99.82	1.45	1.21
1	0.50	0.50	0.47	0.49	94.0	98.00	3.47	3.24
2	1.75	2.75	1.70	2.72	97.14	98.90	3.12	3.01
3	5.50	3.25	5.49	3.23	99.81	99.38	2.96	2.83
4	9.75	6.50	9.68	6.47	99.28	99.53	2.43	2.51
5	10.75	9.25	10.72	9.24	99.72	99.89	1.91	2.25
6	22.25	15.75	22.24	15.71	99.95	99.74	1.64	1.79

References

(S1) S. Thilaga, S. Durga, V. Selvarani, S. Kiruthika and B. Muthukumaran, Multiwalled carbon nanotube supported Pt–Sn–M (M= Ru, Ni, and Ir) catalysts for ethanol electrooxidation, *Ionics*, 2018, **24**, 1721–1731.

(S2) V. Arancibia, M. Valderrama, A. Madariaga, M. C. Zuniga, R. Segura, Extraction of nitrofurantoin and its toxic metabolite from urine by supercritical fluids. Quantitation by high performance liquid chromatography with UV detection. *Talanta*. 2003, **61**, 377–383.

(S3) M. Poulou, P. Macheras, Determination of nitrofurantoin in urine by derivative spectroscopy. *Int. J. Pharmaceut.* 1986, **34**, 29–34.

(S4) P. Thongsrisomboon, B. Liawruangrath, S. Liawruangrath, S. Satienperakul, Determination of nitrofurans residues in animal feeds by flow injection chemiluminescence procedure. *Food Chem.* 2010, **123**, 834–839.

(S5) Y. Wang, T. Chen, Q. Zhuang, Y. Ni, Label-free photoluminescence assay for nitrofurantoin detection in lake water samples using adenosine-stabilized copper nanoclusters as nanoprobes. *Talanta* 2018, **179**, 409–413.

(S6) Z. Cai, S. Pang, L. Wu, E. Hao, J. Rong, Highly sensitive and selective fluorescence sensing of nitrofurantoin based on water-soluble copper nanoclusters. *Spectrochim. Acta A Mol. Biomol. Spectrosc.* 2021, **255**, 119737.

(S7) H. Li, J. Ren, X. Xu, L. Ning, R. Tong, Y. Song, S. Liao, W. Gu, X. Liu, A dual-responsive luminescent metal–organic framework as a recyclable luminescent probe for the highly effective detection of pyrophosphate and nitrofurantoin. *Analyst* 2019, **144**, 4513–4519.

(S8) S. Borse, Z.V. Murthy, T.J. Park, SK. Kailasa, Pepsin mediated synthesis of blue fluorescent copper nanoclusters for sensing of flutamide and chloramphenicol drugs. *Microchem.* 2021, **164**, 105947.

(S9) M.J. Chaichi, S.N. Azizi, M. Heidarpour, A novel luminol chemiluminescent method catalyzed by silver/gold alloy nanoparticles for determination of anticancer drug flutamide. *Spectrochim. Acta A Mol. Biomol. Spectrosc.* 2013, **116**, 594–598.

(S10) S. Esmaeilzadeh, H. Valizadeh, P. Zakeri-Milani, A simple, fast, low cost, HPLC/UV validated method for determination of flutamide: application to protein binding studies. *Adv. Pharm. Bull.* 2016, **6**, 251.

(S11) P.D. Tzanavaras, D.G. Themelis, Automated determination of flutamide by a validated flow-injection method: Application to dissolution studies of pharmaceutical tablets. *J. Pharm. Biomed. Anal.* 2007, **43**, 1820–1824.

(S12) H.R. Salgado, M. De Menezes, M.P. Storti, Determination of flutamide in tablets by high-performance liquid chromatography. *Acta Farmacéutica Bonaerense* 2005, **24**, 246.

(S13) A.A. Khan, A. Khan, A.M. Asiri, S.A. Khan, A. Mohd, Complexation and oxidation of Flutamide with Fe^{3+} and 1, 10-phenanthroline: few analytical applications. *Arab. J. Chem.* 2018, **11**, 240–246.